LETTER TO THE EDITOR

Aperture corrections for disk galaxy properties derived from the CALIFA survey

Balmer emission lines in spiral galaxies

J. Iglesias-Páramo[1,2], J.M. Vílchez[1], L. Galbany[3], S.F. Sánchez[1,2], F.F. Rosales-Ortega[4], D. Mast[2], R. García-Benito[1], B. Husemann[5], J.A.L. Aguerri[6,7], J. Alves[8], S. Bekeraité[5], J. Bland-Hawthorn[9], C. Catalán-Torrecilla[10], A.L. de Amorim[1,11], A. de Lorenzo-Cáceres[6,7], S. Ellis[12], J. Falcón-Barroso[6,7], H. Flores[13], E. Florido[14,15], A. Gallazzi[16,17], J.M. Gomes[18], R.M. González Delgado[1], T. Haines[19], J.D. Hernández-Fernández[20], C. Kehrig[1], A.R. López-Sánchez[12,21], M. Lyubenova[22], R.A. Marino[23], M. Mollá[24], A. Monreal-Ibero[1], A. Mourão[3], P. Papaderos[18], P. Sánchez-Blázquez[25], K. Spekkens[26], V. Stanishev[3], G. van de Ven[22], C.J. Walcher[5], L. Wisotzki[5], S. Zibetti[17], and B. Ziegler[8]

(Affiliations can be found after the references)

ABSTRACT

This work investigates the effect of the aperture size on derived galaxy properties for which we have spatially-resolved optical spectra. We focus on some indicators of star formation activity and dust attenuation for spiral galaxies that have been widely used in previous work on galaxy evolution. We have used 104 spiral galaxies from the CALIFA survey for which 2D spectroscopy with complete spatial coverage is available. From the 3D cubes we have derived growth curves of the most conspicuous Balmer emission lines (Hα, Hβ) for circular apertures of different radii centered at the galaxy's nucleus after removing the underlying stellar continuum. We find that the Hα flux (f(Hα)) growth curve follows a well defined sequence with aperture radius showing low dispersion around the median value. From this analysis, we derive aperture corrections for galaxies in different magnitude and redshift intervals. Once stellar absorption is properly accounted for, the f(Hα)/f(Hβ) ratio growth curve shows a smooth decline, pointing towards the absence of differential dust attenuation as a function of radius. Aperture corrections as a function of the radius are provided in the interval $[0.3, 2.5]R_{50}$. Finally, the Hα equivalent width (EW(Hα)) growth curve increases with the size of the aperture and shows a very large dispersion for small apertures. This large dispersion prevents the use of reliable aperture corrections for this quantity. In addition, this result suggests that separating star-forming and quiescent galaxies based on observed EW(Hα) through small apertures is likely to result in low EW(Hα) star-forming galaxies begin classified as quiescent.

Key words. techniques: spectroscopic - galaxies: evolution - surveys - galaxies: ISM

1. Introduction

The advent of large area surveys has produced an enormous advance in our knowledge of galaxy formation and evolution in recent decades. In particular, those consisting of imaging and single fiber spectroscopy (e.g. 2dFGRS, Folkes et al. 1999; SDSS, York et al. 2000; GAMA, Driver et al. 2011) have provided invaluable information on redshift as well as other galactic properties such as star formation rates (SFR) or metallicities, via the intensities of the most conspicuous emission lines. However, aperture effects are always present in such studies due to the limited (and variable with redshift) coverage of the individual galaxies. Consequently, a fraction of the total flux at all wavelengths is lost and, to date, no recipe to correct for this effect has proved satisfactory, although several studies of aperture effects have been carried out (e.g. Brinchmann et al. 2004; Ellis et al. 2005; Kewley et al. 2005; Salim et al. 2007; Kronberger et al. 2008; Gerssen et al. 2012; Zahid et al. 2013; Hopkins et al. 2013).

In practice, there are two main issues: one is the size of the projection on the sky of the aperture relative to the physical dimensions of the galaxy. The second one, which affects mainly single fiber (or very small aperture) spectrographs (e.g. 2" for

2dFGRS and GAMA; 3" for SDSS), is the precise position of the aperture relative to the galaxy center. This aperture effect has implications for spectral stacking studies, since the fraction of a galaxy covered by a fixed aperture varies with redshift. In this sense, the use of a realistic aperture correction is a *sine qua non* condition in order to carry out the analysis of aperture spectra of galaxies at different epochs, to derive their fundamental properties and to discuss their evolution.

Gerssen et al. (2012) have recently carried out a study of a reduced sample of SDSS star-forming galaxies using the VIMOS integral field spectrograph (Le Fèvre et al. 2003) to map (with full spatial coverage) some properties related to star formation diagnostics. These authors found a large dispersion when comparing their results to color-based SDSS extrapolations. This suggests that full spatial coverage is needed to produce proper corrections for emission lines intensities, and large samples of galaxies covering all the morphological types are required.

The *Calar Alto Legacy Integral Field Area* Survey (CALIFA; Sánchez et al. 2012a) is observing a statistically well-defined sample of 600 galaxies in the local Universe with the Potsdam Multi Aperture Spectrograph (PMAS; Roth et al. 2005) in the PPAK mode. Galaxies have been selected from the SDSS-DR7
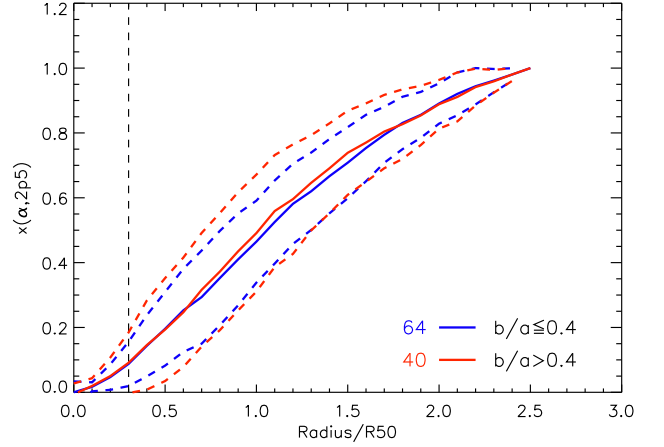
catalog (Abazajian et al. 2009) to fulfill the following conditions: (1) they fall in the redshift range $0.005 < z < 0.03$; and (2) their isophotal diameters in the r' band ($isoA\_r$ in SDSS-DR7) are in the range $45'' < isoA\_r < 80''$. The combination of these three criteria results in a sample of galaxies that fall completely within the PPAK field-of-view with all the relevant emission lines covered with a single spectral setup. The CALIFA galaxies completely sample the color-magnitude diagram down to $M_r = -19$ mag (see Sánchez et al. 2012a). In summary, the data provided by CALIFA are well suited to (a) testing the aperture effects discussed above, thanks to complete spectral and spatial coverage of the sample galaxies, and (b) providing aperture correction factors as a function of aperture size for quantities that vary smoothly with the latter. In our analysis, we adopt the following cosmological parameters: $H_0 = 72$ km s^{-1} Mpc^{-1}, $\Omega_M = 0.27$ and $\Omega_\lambda = 0.73$.

2. Aperture corrections

The basic tools for this process are the CALIFA reduced cubes from the DR1 sample (Husemann et al. 2013). Our starting point is a larger sample containing 258 galaxies including those of DR1 and some others not yet released to the community. The survey sample comprises 24.4% E-S0 and 75.6% Sa-Sm galaxies. We remove those galaxies suspected of being AGN according to several criteria based on optical spectra and radio data following the criteria of Best et al. (2012), Kewley et al. (2001, 2006) and Cid Fernandes et al. (2011). We also removed galaxies with morphological types earlier than S0a since we want to focus only in spiral galaxies. Given that we want to keep only galaxies completely observed within the PPAK field-of-view, we rejected all the galaxies for which $2.5R_{50} \geq 36''$, where R_{50} is the radius containing 50% of the Petrosian flux in the r' band ($petroR50\_r$ in SDSS-DR7). After testing several options like half light radius from circular and elliptical and circular growth curve analysis we decided to use $petroR50\_r$ as our scale as it results in (a) the largest sample of galaxies fulfilling our previous requirements, and (b) the least dispersed profiles for the growth curves to be discussed later. After these considerations, we ended up with a sample of 104 galaxies with morphological types from Sa to Sm completely covered by the PPAK field-of-view. The median values (1σ confidence interval) of the stellar mass, SFR (from dust corrected Hα luminosities), $EW(H\alpha)$ and $f(H\alpha)/f(H\beta)$ distributions of the sample are $\log M^*/M_\odot = 10.25$ ([9.65, 10.85]), $\log SFR/(M_\odot\,yr^{-1}) = 0.45$ ([−0.06, 0.79]), $EW(H\alpha)/\text{Å} = 16.91$ ([6.39, 28.56]) and $f(H\alpha)/f(H\beta) = 4.75$ ([4.00, 5.89]). For each galaxy, we produced stacked spectra by adding the emission from the spaxels within circular apertures centered at the galaxy's nucleus and with radii increasing from 1.5" by steps of 1.5" up to a maximum radius completely covering the hexagonal PPAK aperture. Then we subtracted the stellar continuum to each of our stacked spectra by using the FIT3D code (Sánchez et al. 2011), resulting in a set of spectra of the ionized gas emission. Finally, the fluxes of the emission lines within each aperture were extracted from two independent gaussian fits with the IDL-based routine MPFITEXPR (Markwardt 2009), one for Hβ and another one for the triplet Hα + [N$_{II}$]λ6548,6583Å. A more detailed description on this point will be included in a forthcoming paper.

3. Results

We illustrate our results with the aperture corrections for three observables: $f(H\alpha)$, the $f(H\alpha)/f(H\beta)$ ratio, and the $EW(H\alpha)$,

Fig. 1. Growth curve of $f(H\alpha)$ normalized to $f(H\alpha)$ at $2.5R_{50}$, $x(\alpha, 2p5)$, as a function of the radius of the aperture. Bold red (blue) lines correspond to the median values for galaxies with $b/a > 0.4$ ($b/a < 0.4$). Dashed red and blue lines correspond to 1σ deviations from the median curve. Numbers indicate the size of each subsample. The vertical dashed line corresponds to $0.3R_{50}$, which on average corresponds to the FWHM of the CALIFA psf for our sample.

shown in figures 1 to 3. The figures show the median profiles of the growth curves corresponding to these three quantities normalized to the value measured within an external isophote containing most of the optical light of the galaxy. We normalized the profiles to the value measured at $2.5R_{50}$ since this is the typical value covered by the PPAK field-of-view for the CALIFA sample. This aperture, $2.5R_{50}$, encloses on average $\simeq 90\%$ of the total Hα flux of spiral galaxies[1].

Figure 1 shows the median $f(H\alpha)$ growth curve normalized to $f(H\alpha)$ at $2.5R_{50}$, $x(\alpha, 2p5)$. We have split our sample according to the axis ratio in order to take into account the effect that the inclination of the galaxy may have on the values measured through circular apertures. For this, we use the isophotal axis in the r' band $isoA\_r$ and $isoB\_r$ from SDSS-DR7. This choice gives average values of $\langle isoB\_r/isoA\_r \rangle = 0.27$ and 0.53 respectively for each subsample. We have verified that other choices like the semi-minor to semi-major axis from elliptical growth curve and light momentum analysis yield basically the same average inclination distributions as our selection. As it can be seen, the average curves for both ranges of inclination are quite similar within the 1σ uncertainties. The low thickness of the ionized gas disks, as estimated from the low velocity dispersion of the H$_{II}$ regions ($\approx 10\ km\ s^{-1}$, Relaño et al. 2005), suggests that no important differences in the Hα growth curves of face-on and edge-on galaxies should be expected. However, a circular aperture covers different parts of the disk for face-on and edge-on galaxies. Thus, the similarity found for both curves could be partly due to the fact that the average inclination values of our subsamples are far from the extreme face-on and edge-on cases and close enough from each other, although we have verified that even the curves restricted to galaxies with the most extreme values in our sample are not significantly different from each other. A physi-

---

[1] Estimated by adding up the contribution to the Hα emission flux of all the spaxels of the PPAK aperture for each galaxy of the sample. This must be taken as a rough estimation since the largest galaxies in the sample show Hα emission beyond the PPAK aperture.

Table 1. $x(\alpha, 2p5)$ and $x(\alpha\beta, 2p5)$ and their 1σ deviations as a function of the size of the circular aperture normalized to R_{50}.

r/R_{50}	$x(\alpha, 2p5)$	(σ)	$x(\alpha\beta, 2p5)$	(σ)
0.3	0.091	(0.074)	1.078	(0.221)
0.5	0.194	(0.119)	1.052	(0.240)
0.7	0.301	(0.156)	1.042	(0.234)
0.9	0.419	(0.158)	1.034	(0.163)
1.1	0.530	(0.146)	1.028	(0.136)
1.3	0.629	(0.130)	1.021	(0.145)
1.5	0.718	(0.117)	1.026	(0.154)
1.7	0.798	(0.101)	1.020	(0.093)
1.9	0.854	(0.079)	1.009	(0.088)
2.1	0.917	(0.070)	1.009	(0.129)
2.3	0.961	(0.039)	1.003	(0.086)
2.5	1.000	–	1.000	–

Table 2. Redshift and absolute magnitude ranges at which the aperture corrections listed in table 1 are valid for SDSS and SAMI data.

Redshift	Absolute magnitude range	
	SDSS	SAMI
0.02	$-18 \lesssim M_r$	$-22.5 \lesssim M_r \lesssim -16.5$
0.04	$-20.5 \lesssim M_r$	$-22 \lesssim M_r \lesssim -18.5$
0.06	$-21.5 \lesssim M_r \lesssim -16$	$M_r \lesssim -20$
0.08	$-22 \lesssim M_r \lesssim -16.5$	$M_r \lesssim -21$
0.10	$-22.5 \lesssim M_r \lesssim -17$	$M_r \lesssim -21.5$
0.14	$-22.5 \lesssim M_r \lesssim -18$	
0.18	$-22.5 \lesssim M_r \lesssim -19$	

cally motivated study of the Hα spatial distribution for face-on and edge-on galaxies is out of the scope of this work and will be part of ongoing work devoted to the SFR in CALIFA galaxies. Similarly, aperture corrections as a function of Hubble type require a larger sample and will be part of future papers on this topic. We list in table 1 the median growth curve and the 1σ uncertainties of $f(\text{H}\alpha)$ as a function of the aperture radius. Given that galaxies with low and high inclination show very similar results, these values correspond to our complete working sample.

An issue that deserves discussion is the effect of the FWHM of the CALIFA psf (~ 3.6") on the growth curves of the emission lines. It was demonstrated by Trujillo et al. (2001) that the parameters of a Sérsic profile are affected by the seeing. For exponential disks, which correspond to a $n = 1$ profile, the central intensity and effective radius are recovered within 20% of their true value disregarding the ellipticity as far as $FWHM/r_{eff} \leq 0.3$. This result prevents the use of aperture corrections below this limit since they could be severely affected by seeing. Given that the average value of R_{50} for our sample is ≈ 10", the range of validity of our aperture correction is valid for radii $r/R_{50} \gtrsim 0.3$. A further limitation is the fact that the observed size of the galaxies decreases as we move to higher redshifts, and this imposes both a lower and an upper limit to the range of magnitudes for which our correction can be applied. Based on average measurements of R_{50} for spiral galaxies from SDSS, we have derived the validity ranges of the aperture corrections at different redshifts. In table 2, we show these ranges for two representative projects providing spectra with different aperture sizes: SDSS (single-fiber, $\varnothing = 3$") and SAMI (multi-fiber bundle, $\varnothing = 15$", Bryant et al 2011). In both cases the lower and upper magnitude limits correspond to the magnitudes at which $r_{aper}/R_{50} \geq 0.3$ and $r_{aper}/R_{50} \leq 2.5$ respectively[2] based on their average sizes at the different redshift proved with a sample of SDSS-DR7 galaxies. The applicability of the aperture corrections is meaningful for individual galaxies within the limits listed in table 2, thus average corrections to large sample of galaxies in order to correct quantities like the star formation density from observed Hα luminosities are not recommended.
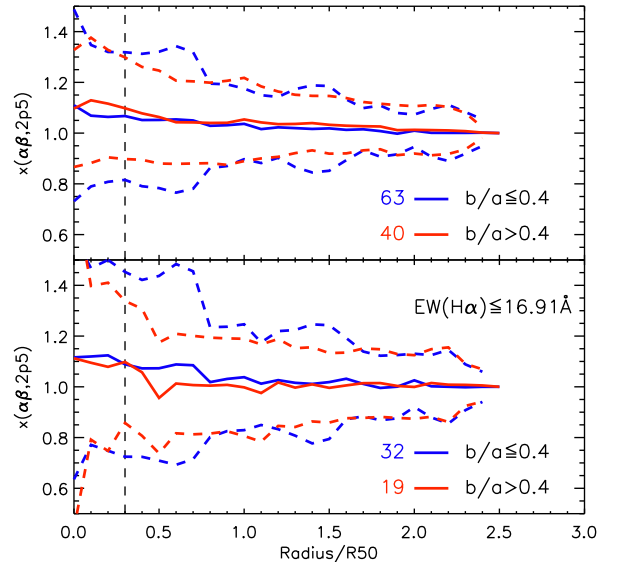
[2] There is a further restriction to the upper magnitude limit due to the effect of the psf on the determination of R_{50}. This upper limit corresponds to the magnitude at which $FWHM \approx R_{50}$ and it must apply when it is more restrictive than the one given in table 2 for each redshift. In the particular case of SDSS images, R_{50} are not corrected for the psf such that this limit can become relevant at high redshifts. A discussion on the limits of reliability of R_{50} at different redshifts can be found in González-Pérez et al. (2011).
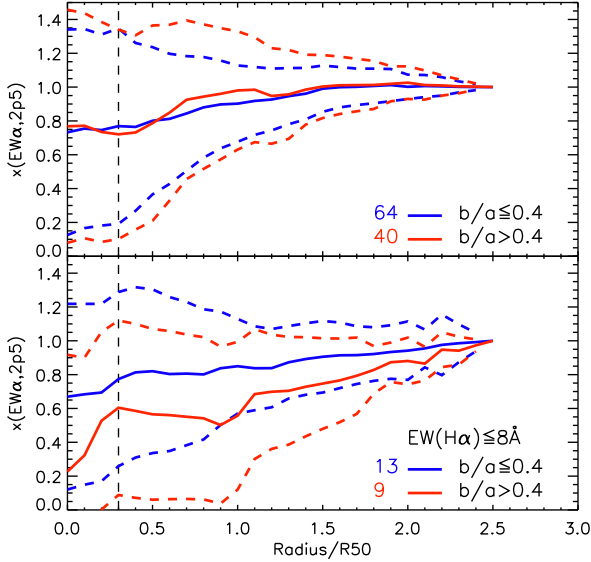
Figure 2 (top panel) shows the median $f(\text{H}\alpha)/f(\text{H}\beta)$ ratio growth curve normalized to $2.5R_{50}$, $x(\alpha\beta, 2p5)$, again split for low and high inclination galaxies. Both curves show a smooth decline from a central value of $\simeq 1.1$ down to 1.0 at the normalization radius, and no significant difference with the inclination of the galaxies. The median growth curve and the 1σ uncertainty for the whole sample are listed in table 1. The very smooth decline of $x(\alpha\beta, 2p5)$ supports the earlier result that the dust attenuation shows little dependence with the radial distance (Sánchez et al. 2012b). We examined the effect of non-negligible residual Hβ absorption after subtraction of the underlying stellar continuum by restricting the analysis to galaxies with $EW(\text{H}\alpha) \leq 16.9$Å (see lower panel of Fig. 2). It can be seen that this growth curve is consistent within the uncertainties with the corresponding to the whole sample, what suggests that our Hβ fluxes, and thus the $f(\text{H}\alpha)/f(\text{H}\beta)$ ratio, are on average free from this effect.

Figure 3 (top panel) shows the median $EW(\text{H}\alpha)$ growth curve, $x(EW\alpha, 2p5)$, which as in previous cases is similar for galaxies with low and high inclination. This curve grows with radius, ranging from a central value of $\simeq 0.7$ to 1 at the normal-

Fig. 2. Top: Growth curve of $f(\text{H}\alpha)/f(\text{H}\beta)$ normalized to $f(\text{H}\alpha)/f(\text{H}\beta)$ at $2.5R_{50}$, $x(\alpha\beta, 2p5)$, as a function of the radius of the aperture. Lines and colors as in figure 1. For one of the galaxies the Hβ emission line was not detected in all the apertures and it was not included. **Bottom:** Same as top panel restricted to galaxies with $EW(\text{H}\alpha) \leq 16.91$Å.

3

Fig. 3. Top: Growth curve of $EW(H\alpha)$ normalized to $EW(H\alpha)$ at $2.5R_{50}$, $x(EW\alpha, 2p5)$, as a function of the radius. **Bottom:** Same as top panel restricted to the galaxies with $EW(H\alpha) \leq 8\text{Å}$ at $2.5R_{50}$.

ization radius. It is remarkable the large dispersion of this quantity measured at small apertures ($\sigma > 0.3$ at $r/R_{50} \leq 1.3$). The observed dispersion at small radii is due to the fact that $EW(H\alpha)$ is an intensive quantity (contrarily to $H\alpha$ or $H\beta$ fluxes which are extensive quantities), and thus very low or high values at small radii can be measured due to the presence of features like circumnuclear rings of star formation or nuclear starbursts respectively. This large dispersion at small radii prevents the use of a reliable aperture correction for the $EW(H\alpha)$. The main implication of the large dispersion at small radii is the possibility that star-forming galaxies observed through a small aperture are misclassified as quiescent if the classification is based only in an extrapolation of the central value of $EW(H\alpha)$. To illustrate this we show in the bottom panel of figure 3 $x(EW\alpha, 2p5)$ as a function of radius restricted to galaxies with $EW(H\alpha) \leq 8\text{Å}$. The curve of the low-inclination galaxies is clearly below that of the high-inclination ones, which follows a trend similar to that of the whole sample. As an example, according to this plot a face-on spiral galaxy with (total) $EW(H\alpha) = 6\text{Å}$ and observed through an aperture covering less than R_{50} will have $\simeq 50\%$ chance of showing (observed) $EW(H\alpha) \leq 3\text{Å}$, and thus being classified as quiescent depending on the adopted limit (previous works separate active and quiescent galaxies at $EW(H\alpha) \simeq 2 - 4\text{Å}$, see Cid Fernandes et al. 2010). This effect is less dramatic for edge-on galaxies.

We conclude that the median $f(H\alpha)$ growth curve of spiral galaxies is well defined and shows a low dispersion for a range of aperture sizes between $0.3R_{50}$ and $2.5R_{50}$. The $f(H\alpha)/f(H\beta)$ ratio growth curve presents a smooth behavior suggesting low dependence of the dust attenuation with radius. Median aperture corrections for this quantity are also meaningful. The observed large dispersion around the median $EW(H\alpha)$ growth curve prevents the derivation of a reliable aperture correction especially at small radii. This large dispersion warns about the use of the $EW(H\alpha)$ as the criterion to classify star-forming and quiescent galaxies for which the size of the aperture is $\lesssim R_{50}$ since it might result in misclassification of low $EW(H\alpha)$ galaxies. We end up

by adding that this paper presents only the tip of the iceberg. Aperture effects are widely mentioned but rarely understood. Their influence can seriously affect scientific results through systematic error (Bland-Hawthorn et al 2011). Forthcoming papers will be devoted to providing a complete set of diagnostics involving other indicators of SFR and/or abundances, and to applying these results to existing datasets.

References

Abazajian, K. N., Adelman-McCarthy, J. K., Agüeros, M. A., et al. 2009, ApJS, 182, 543
Best, P. N., & Heckman, T. M. 2012, MNRAS, 421, 1569
Bland-Hawthorn, J., Bryant, J., Robertson, G., et al. 2011, Optics Express, 19, 2649
Brinchmann, J., Charlot, S., White, S. D. M., et al. 2004, MNRAS, 351, 1151
Bryant, J. J., O'Byrne, J. W., Bland-Hawthorn, J., & Leon-Saval, S. G. 2011, MNRAS, 415, 2173
Cid Fernandes, R., Stasińska, G., Schlickmann, M. S., et al. 2010, MNRAS, 403, 1036
Cid Fernandes, R., Stasińska, G., Mateus, A., & Vale Asari, N. 2011, MNRAS, 413, 1687
Driver, S. P., Hill, D. T., Kelvin, L. S., et al. 2011, MNRAS, 413, 971
Ellis, S. C., Driver, S. P., Allen, P. D., et al. 2005, MNRAS, 363, 1257
Folkes, S., Ronen, S., Price, I., et al. 1999, MNRAS, 308, 459
Gerssen, J., Wilman, D. J., & Christensen, L. 2012, MNRAS, 420, 197
González-Pérez, V., Castander, F. J., & Kauffmann, G. 2011, MNRAS, 411, 1151
Hopkins, A. M., Driver, S. P., Brough, S., et al. 2013, MNRAS, 700
Husemann, B., Jahnke, K., Sánchez, S. F., et al. 2013, A&A, 549, A87
Kewley, L. J., Dopita, M. A., Sutherland, R. S., Heisler, C. A., & Trevena, J. 2001, ApJ, 556, 121
Kewley, L. J., Jansen, R. A., & Geller, M. J. 2005, PASP, 117, 227
Kewley, L. J., Groves, B., Kauffmann, G., & Heckman, T. 2006, MNRAS, 372, 961
Kronberger, T., Kapferer, W., Unterguggenberger, S., Schindler, S., & Ziegler, B. L. 2008, A&A, 483, 783
Le Fèvre, O., Saisse, M., Mancini, D., et al. 2003, Proc. SPIE, 4841, 1670
Markwardt, C. B. 2009, Astronomical Data Analysis Software and Systems XVIII, 411, 251
Relaño, M., Beckman, J. E., Zurita, A., Rozas, M., & Giammanco, C. 2005, A&A, 431, 235
Roth, M. M., Kelz, A., Fechner, T., et al. 2005, PASP, 117, 620
Salim, S., Rich, R. M., Charlot, S., et al. 2007, ApJS, 173, 267
Sánchez, S. F., Rosales-Ortega, F. F., Kennicutt, R. C., et al. 2011, MNRAS, 410, 313
Sánchez, S. F., Kennicutt, R. C., Gil de Paz, A., et al. 2012a, A&A, 538, A8
Sánchez, S. F., Rosales-Ortega, F. F., Marino, R. A., et al. 2012b, A&A, 546, A2

Trujillo, I., Aguerri, J. A. L., Cepa, J., & Gutiérrez, C. M. 2001, MNRAS, 321, 269

York, D. G., Adelman, J., Anderson, J. E., Jr., et al. 2000, AJ, 120, 1579

Zahid, H. J., Yates, R. M., Kewley, L. J., & Kudritzki, R. P. 2013, ApJ, 763, 92

[1] Instituto de Astrofísica de Andalucía - CSIC, 18008 Granada, Spain

[2] Centro Astronómico Hispano Alemán, 04004 Almería, Spain

[3] CENTRA Centro Multidisciplinar de Astrofísica, Instituto Superior Técnico, Av. Rovisco Pais 1, 1049-001 Lisbon, Portugal

[4] Instituto Nacional de Astrofísica, Óptica y Electrónica, Luis E. Erro 1, 72840 Tonantzintla, Puebla, Méjico

[5] Leibniz-Institut für Astrophysik Potsdam (AIP), An der Sternwarte 16, 14482 Potsdam, Germany

[6] Instituto de Astrofísica de Canarias, Vía Láctea s/n, La Laguna, Tenerife, Spain

[7] Departamento de Astrofísica, Universidad de La Laguna, 38205 La Laguna, Tenerife, Spain

[8] University of Vienna, Department of Astrophysics, Türkenschanzstr. 17, 1180 Vienna, Austria

[9] Sydney Institute for Astronomy, School of Physics A28, University of Sydney, NSW 2006, Australia

[10] Departamento de Astrofísica y CC. de la Atmósfera, Universidad Complutense de Madrid, 28040 Madrid, Spain

[11] Departamento de Física, Universidade Federal de Santa Catarina, PO Box 476, 88040-900 Florianpolis, SC, Brazil

[12] Australian Astronomical Observatory, 105 Delhi Rd., North Ryde, NSW 1670, Australia

[13] GEPI, Observatoire de Paris, CNRS-UMR8111, Univ. Paris-Diderot, 5 place Janssen, 92195 Meudon, France

[14] Departamento de Física Teórica y del Cosmos, University of Granada, Facultad de Ciencias (Edificio Mecenas), 18071 Granada, Spain

[15] Instituto Carlos I de Física Teórica y Computación, 18071 Granada, Spain

[16] Dark Cosmology Centre, Niels Bohr Institute, University of Copenhagen, Juliane Mariesvej 30, 2100 Copenhagen, Denmark

[17] INAF Osservatorio Astrofisico di Arcetri Largo Enrico Fermi, 5 50125 Firenze, Italy

[18] Centro de Astrofísica and Faculdade de Ciências, Universidade do Porto, Rua das Estrelas, 4150-762 Porto, Portugal

[19] Department of Physics and Astronomy University of Missouri Kansas City, Kansas City, MO 64110, USA

[20] Departamento de Astronomia do Instituto de Astronomia, Geofísica e Ciências Atmosféricas da USP, Rua do Matão 1226, Cidade Universitária, 05508-090, São Paulo, Brasil

[21] Department of Physics and Astronomy, Macquarie University, NSW 2109, Australia

[22] Max-Planck-Institut für Astronomie, Königstuhl 17, 69117 Heidelberg, Germany

[23] CEI Campus Moncloa, UCM-UPM, Departamento de Astrofísica y CC. de la Atmósfera, Facultad de CC. Físicas, Universidad Complutense de Madrid, Avda. Complutense s/n, 28040 Madrid, Spain

[24] Departamento de Investigación Básica, CIEMAT, Avda. Complutense 22, 28040 Madrid, Spain

[25] Departamento de Física Teórica, Universidad Autónoma de Madrid, 28049 Madrid, Spain

[26] Department of Physics, Royal Military College of Canada, PO Box 17000, Station Forces, Kingston, Ontario, K7K 7B4, Canada